# Ultrasensitive binder-free glucose sensors based on the pyrolysis of in situ grown Cu MOF

**Xuan Zhang [a], Jiangshui Luo [a,b*], Pengyi Tang[c,d], Joan Ramon Morante[d], Jordi Arbiol[c,e*], Cailing Xu[f], Qingfeng Li[b], Jan Fransaer[a*]**

*Keywords:* metal-organic frameworks, electrodeposition, carbon-metal composite materials, glucose sensors.

[a]Department of Materials Engineering, KU Leuven, Leuven 3001, Belgium. E-mail: jan.fransaer@mtm.kuleuven.be; jiangshui.luo@kuleuven.be

[b]Department of Energy Conversion and Storage, Technical University of Denmark, Kgs. Lyngby 2800, Denmark.

[c]Catalan Institute of Nanoscience and Nanotechnology (ICN2), CSIC and The Barcelona Institute of Science and Technology (BIST), Campus UAB, Bellaterra, 08193 Barcelona, Catalonia, Spain. E-mail: arbiol@icrea.cat

[d]Catalonia Institute for Energy Research (IREC), Jardins de les Dones de Negre 1, Sant Adrià del Besòs, 08930 Barcelona, Catalonia, Spain

[e]ICREA, Pg. Lluís Companys 23, 08010 Barcelona, Catalonia, Spain

[f]Key Laboratory of Nonferrous Metal Chemistry and Resources Utilization of Gansu Province, College of Chemistry and Chemical Engineering, Lanzhou University, Lanzhou 730000, China.

**Abstract**

A non-enzymatic glucose sensor based on carbon/Cu composite materials was developed by the in-situ growth and subsequent pyrolysis of metal-organic frameworks (MOFs) on Cu foam. After pyrolysis, SEM, HRTEM and STEM-EELS were employed to clarify the hierarchical Cu@porous carbon electrode. It is found that the Cu nanoparticles are uniformly embedded in the carbon matrix, attached on the carbon layer closely. The electrocatalytic activity of the Cu@porous carbon matrix electrode for glucose sensing was explored by cyclic voltammetry (CV) and chronoamperometry. The resulting Cu@porous carbon matrix electrode displays ultrahigh sensitivity (10.1 mA $cm^{-2}$ $mM^{-1}$), low detection limit (< 1 μM), short response time (less than 2 s) and good stability, indicating that the developed electrode is a promising candidate material for glucose sensors.

## Introduction

Diabetes has become one of the biggest health problems in the world with more than 370 million people affected.[1] Currently, glucose sensors constitute 85% of the market share of all biosensor products for detecting diabetes. As more and more people are affected by diabetes, a safe, efficient and noninvasive ultra-sensitive glucose monitoring biosensor is a way to improve patient's adherence and health. Therefore, the development of better and cheaper glucose sensors has drawn a lot of attention.[2–4] Because traditional enzyme-based biosensors are easily affected by temperature, pH and humidity, glucose sensors based on transition metals (Pt, Au, Ag, Cu, Ni, Fe, Co, Mn, etc.) as well as their oxides and sulfides in alkaline solutions have been extensively explored as promising candidates for next-generation glucose sensors.[5–12] Among these materials, Cu (or CuO) is an interesting material for glucose sensor due to the fact that it is inexpensive, non-toxic and environmentally stable. More importantly, the electrochemical glucose oxidation shows fast kinetics on Cu (or CuO).[13, 14]

It is well known that the electrocatalytic active surface area plays a critical role in enzymeless analysis. In order to increase the electrocatalytic active surface area, encouraging results have been shown by Cu nanomaterials (nanoparticles, nanocluster, nanobelts, nanocubes, etc.) for glucose sensors recently.[15–19] Moreover, in order to avoid the aggregation of nanomaterials and enhance the catalytic activity of Cu materials, great efforts have been made to combine copper or copper oxides with carbon-based nanomaterials such as carbon nanotubes and graphene. For example, Ding et al. synthesized copper nanoparticles (NPs) decorated nitrogen-doped graphene (Cu-N-G) by thermal treatment. Compared with pure Cu NPs, the Cu-N-G showed enhanced electrocatalytic activity for the glucose oxidation (*e.g.* the oxidation peak current increased a lot).[20] Nevertheless, in the typical fabrication process of glucose sensor, the polymer binders such as Nafion, polyvinylidene fluoride (PVDF) or chitosan are used to immobilize active materials. These binders have been shown to increase

the electrical resistance, hinder the electrolyte diffusion and decrease the effective active surface area.[21–23]Thus, researchers focus on in-situ synthesis of nanostructured Cu directly on the substrate. For instance, Li et al. successfully prepared free-standing porous CuO nanowire electrodes on a Cu foil. The in-situ engineered electrodes show higher sensitivity than "reconstituted" electrodes (electroactive materials that are pasted on an electrode with the addition of a binder).[13] Furthermore, Zhang et al. used Cu foam as the precursor for in-situ growth of CuO nanowires by anodic electrodeposition.[24] However, the preparation of electrodes based on binder-free carbon/Cu composite materials remains challenging.

Metal-organic frameworks (MOFs) are highly porous coordination polymers formed by combining organic linkers and metal ions. Due to their unique structures, nano-scale cavities and open channels, MOFs are considered promising candidates for synthesizing porous carbon materials and nano-sized metal particles.[25–31] Very recently, a new method patented by BASF proposed the electrochemical synthesis of MOFs, avoiding the use of salts and saving synthesis time.[32] Besides, Ameloot et al. reported that densely packed crystalline Cu-based MOF layers could be synthesized on pure copper electrodes by anodic electroprecipitation.[33] Furthermore, the of the electrochemical nucleation and growth of HKUST-1 layers have been proposed by our group.[34]

Taking the above considerations into account, we propose a facile method to prepare binder-free electrodes based on carbon/Cu composite materials (**Figure 1**). Firstly, the archetypal MOF HKUST-1 (Cu-BTC) was directly grown on a copper foam by anodic electroprecipitation. After pyrolysis, the Cu nanoparticles embedded in the porous carbon matrix (Cu@porous carbon material) were successfully fabricated on the Cu foam. The resulting Cu@porous carbon matrix electrode was tested as a non-enzymatic electrochemical glucose sensor electrode. The Cu@porous carbon matrix electrode displayed much better electrochemical catalytic performance towards glucose than Cu foam and flat copper electrodes.

## 2. Results and discussions

HKUST-1 was successfully deposited on the copper foam substrate, as shown by the XRD pattern of materials scratched from the substrate (**Figure S1**). The characteristic peaks of Cu-BTC framework at $2\theta \approx 9.5°$, 11.5° and 13.4° can be clearly identified, which agree well with previous literature.[35] Furthermore, HKUST-1 can be deposited on different copper substrates such as plate (**Figure 2a**), wire (**Figure 2b**) and foam (**Figure 2c**). The HKUST-1 grows conformably on the surface of the different copper substrates. This advantage can meet the need of commercial electronic devices. In this work, we choose copper foam as the substrate because the 3D structure of the copper foam provides high surface area (based on same geometry area), which will increase the sensitivity. At higher magnification, the typical octahedral morphology of HKUST-1 can be observed (inset of **Figure 2c**). The crystal sizes range from 2 μm to 8 μm. The result of EDS is illustrated in **Figure. S2**, confirming the existence of C, O and Cu (from HKUST-1) and Pt (from Pt sputtered for SEM imaging). After pyrolysis, the "octahedral unit" remains while the pyrolized MOF still covers the surface of the copper foam (**Figure 3**). The pyrolytic carbon is expected to act as an electron pathway between the copper nanoparticles and the copper substrate. According to thermogravimetric analysis (TGA) (**Figure S3**), there are three main weight loss events during pyrolysis. Events A and B probably correspond to the loss of guest molecules of ethanol (b.p. = 78 ℃) and DMF (b.p. = 153 °C), respectively. After that, there is a plateau (event C) from 210 ℃ to 250 ℃, indicating that the framework of HKUST-1 is stable up to 250 °C. Event D starts from 250 °C and is attributed to the thermal decomposition of the linker molecules. After the thermal decomposition, copper particles can be found dispersed on the surface. Most copper particles are below 300 nm (**Figure 3c** and **3d**). However, there are some large Cu particles on the surface of the porous carbon matrix. These particles probably arise from outer surface decomposition of MOF units, especially for the overlap of MOF units as shown in **Figure 2c**. This phenomenon has been observed before by Song et al.

as well.[28] The EDS measurements (**Figure S4**) confirm three elements: C from the carbon matrix, Cu from nanoparticles and O from the CuO thin layer (oxidized in the air), respectively. These results are in good agreement with the XRD measurement results. As shown in **Figure S5**, three characteristic peaks for Cu were observed at $2\theta$ = 43.3°, 50.4° and 74.2°, corresponding to Miller indices (111), (200) and (220), respectively. Moreover, a small peak at $2\theta$ = 36.8° can be clearly observed, which corresponds to (111) reflection peak of cubic CuO phase.[36,37] In addition, the SEM micrographs of the Cu foam, HKUST-1-covered and Cu@porous carbon matrix electrodes (**Figure S6**) show that the Cu@porous carbon matrix is in close contact with the Cu foam.

To further explore the structure of single nanoparticles, TEM and STEM-EELS mappings have been conducted. As shown in Figure 4 (a), the nanoparticles are supported by carbon sheets. HRTEM analysis and corresponding reduced FFT (fast Fourier transform) spectra (**Figure 4b**, **4c** and **4d**) show that the species are a mixture of cubic CuO ([FM3-M]-Space group 225, with lattice parameters of a = 0.4245 nm, and α = 90° as visualized along the [112] direction), and Cu ([I4/MMM]-Space group 139, with lattice parameters of a = 0.2892 nm, and α = 90°), which perfectly agree with the XRD observations (**Figure S5**). The RGB composition of IFFT (Inverse fast Fourier transform) from CuO and Cu further confirms the HRTEM analysis (**Figure 4e**). To figure out the chemical composition of Cu@porous carbon matrix materials, STEM-EELS has been conducted (**Figure 5**). The general view and magnified details of the HAADF-STEM images are displayed in **Figure 5**, which also show that the nanoparticles are supported by carbon sheets. The geometrical shape of the nanoparticles is spherical. Moreover, the relative compositions of Cu, O and C elements of these nanoparticles have been mapped by means of EELS analysis using Hartree-Slater model for signal quantification and power law for background removal.[38] Clearly, the nanoparticle is embedded in the carbon layer. Around the outer shell of the nanoparticles, there is a thin layer with a relatively high O concentration, which is probably due to the oxidation of the Cu

nanoparticles in air.[39] In addition, Cu dominates the main region of the nanoparticles. These results are in good agreement with EDS (**Figure S4**), TEM (**Figure 4**) and XRD observations (**Figure S5**). After glucose sensor performance tests, the structure and chemical compositions of the Cu@porous carbon matrix materials were analyzed again by TEM and STEM-EELS composition maps extracted from the obtained spectrum images (SIs). It was found that after the performance test, the nanoparticles were still attached to the carbon layer (**Figure 6a**). After the tests, the structure of the nanoparticles changed to urchin-like particles, which is probably caused by the electrochemical oxidation of Cu into CuO. A similar change has been observed before for the transformation of $Cu_2O$ into CuO nanostructures.[40] However, the hierarchical structure of the nanoparticles embedded in the carbon matrix units remains unchanged (**Figure S7a**). The HRTEM and corresponding reduced FFT spectra (**Figure 6b**, **6c** and **6d**) indicate that the nanoparticle crystallizes in the form of a cubic CuO phase ([FM3-M]-Space group 225, with lattice parameters of a = 0.4245 nm, and α = 90° as visualized along the [011] direction). Furthermore, the relative O content of the particles increased significantly due to the presence of cubic CuO phase after the sensor test (**Figure 6e**), which is confirmed by EDS results (**Figure S7b**). It is worth noting from the relative C content of the nanoparticles that each particle is covered by a thin carbon layer and connected by a carbon layer to each other. This unique behavior might be the reason for the transport of charge and the protection of the nanoparticles from aggregation and degradation during glucose oxidation. Combining XRD patterns (**Figure S5**), TEM observations (**Figure 4**, **5** and **6**) and the electrochemical information (as shown in **Figures 7** and **8**) of Cu@porous carbon matrix materials for the glucose sensor the possible electro-oxidation mechanism of glucose on the Cu@porous carbon matrix surface in an alkaline solution can be assumed as follows: [41, 42]

$$Cu + 2OH^- - 2e^- \rightleftharpoons Cu(OH)_2 \quad (1)$$

$$Cu(OH)_2 + OH^- \rightleftharpoons CuOOH + H_2O + e^- \quad (2)$$

$$CuOOH + e^- + \text{glucose} \longrightarrow CuO + OH^- + \text{gluconic acid} \quad (3)$$

$$CuO + OH^- \rightleftharpoons CuOOH + e^- \quad (4)$$

The reactions (1) and (2) occur in activated process before test. After addition of glucose, the oxidative Cu(III) could catalyze glucose oxidation to generate gluconolactone and then gluconolactone is further oxidized to glucose acid. The reaction catalyzed by Cu@porous carbon matrix electrode was assisted by the Cu(II)/Cu(III) redox couple.

The CV curves of the Cu@porous carbon matrix electrode in 0.1 M NaOH with different concentrations of glucose at a scan rate of 50 mV $s^{-1}$ is shown in **Figure 7a**. In the absence of glucose (curve A), there is no obvious oxidation peak. When glucose was added to the 0.1 M NaOH solution, a clear increase of the oxidative peak current was observed in the potential range between +0.4 V and +0.7 V (*vs*. Hg/HgO), corresponding to the irreversible oxidation of glucose. The optimal detection potential was determined from the amperometric responses of the Cu@porous carbon matrix electrode at different potentials from +0.45 to +0.65 V with the addition of 1 mM glucose (**Figure 7b**). The Cu@porous carbon matrix electrode shows only a slightly lower current response at +0.55 V than +0.6 V. However, at higher potentials the influence of interferences and polarization of the oxygen evolution are larger. Therefore, the potential is subsequently fixed at +0.55 V for amperometric *i-t* tests. The amperometric responses of the Cu plate, Cu foam and Cu@porous carbon matrix electrode to 1 mM glucose at +0.55 V in 0.1 M NaOH are shown in **Figure 7c**. The copper foam shows a 100% increase in current compared to the copper plate due to its larger surface area. The current response of the Cu@porous carbon matrix decorated copper foam is in turn 70% larger compared to the bare copper foam.

**Figure 8a** displays an amperometric *i-t* test measured in 0.1 M NaOH at +0.55 V under stepwise addition of glucose. When the current was stable, different concentrations of glucose solutions were successively injected into the solution under stirring, which induced an increase in the current within 2 s. The low-concentration part is magnified and shown in the

inset above the amperometric *i-t* curve. Another inset is the amperometric response of the Cu@porous carbon matrix electrode to the addition of 1 μM and 2.5 μM glucose solutions. An increase of current can be clearly identified even for 1 μM glucose. Moreover, as shown in Figure S8, the Cu@porous carbon matrix decorated copper foam shown much larger current response for 10 μM glucose than bare copper foam or copper plate. Besides, we cannot observe an increase in current for the bare copper foam or copper plate electrode with the addition of 1 μM of glucose. The calibration curves based on the results of the amperometric *i-t* test is presented in **Figure 8b**. The current ($i$) is correlated with the glucose concentration ($c$) in the range of 1 μM − 6000 μM with a correlation coefficient of 0.9998 using the following equation: [43]

$$i = \frac{12.1\mathrm{c}}{928.9 + c} \tag{5}$$

Between 1 μM and 300 μM glucose, the response is linear ($R^2$ = 0.9947) as shown in the inset of **Figure 8b**. In this concentration range (linear part), the sensitivity is 10.1 mA $cm^{-2}$ $mM^{-1}$ in term of geometrical area. To our best knowledge, this current response is the highest among all reported non-enzymatic glucose sensors as indicated in **Figure 9**.

As there are various oxidizable species present in human blood, such as uric acid (UA), ascorbic acid (AA), sucrose, fructose, the ability to discriminate these interferences is an important factor for glucose sensors. Under stepwise addition of the same amount (0.1 mM) of glucose, UA, AA, sucrose, fructose, the interferences showed obvious current responses as shown in curve A (**Figure 10a**). However, when the concentration of the interferences was decreased from 0.1 mM to 0.01 mM, almost no current response can be observed for species other than glucose (curve B, **Figure 10a**). In human blood, the concentration of these interferences are much smaller (< 1/30) than the concentration of glucose.[43, 44] Therefore, when adding the interferences in biologically relevant concentrations, after the addition of 0.1 mM glucose, there is no current response from the interferences (curve C, **Figure 10a**).

These results suggest that the Cu@porous carbon matrix electrode could be a good sensing material for blood samples. Furthermore, the stability of the Cu@porous carbon matrix electrode was investigated by recording the continuous or intermittent amperometric responses to 0.1 mM glucose. The longtime current response of the Cu@porous carbon matrix electrode indicates that around 89% can be retained during a period of 1800 s (**Figure 10b**). Furthermore, after storage at room temperature in ambient atmosphere for 25 days, the sensitivity of the electrode decreased only slightly compared with its initial response as shown in the inset of **Figure 10b**.

## 3. Conclusions

In summary, HKUST-1 can be easily synthesized on the different kinds of copper substrates. After pyrolysis, carbon-Cu composite materials can be grown in-situ on the Cu foam. The resulting electrode shows high sensitivity, low detection limit and good stability for the non-enzymatic detection of glucose. The excellent electrochemical performance of the Cu@porous carbon matrix electrode can be attributed to the multidimensional hierarchical structure of the electrode and the synergistic effect between Cu and carbon. These results indicate that the Cu@porous carbon matrix electrode could be a promising candidate for the construction of non-enzymatic glucose sensors, especially for saliva-based glucose sensors due to the very high sensitivity.

## 4. Experimental section

*Electrodeposited MOF*: All reagents were of analytical purity and used as received without further purification. Three kinds of copper substrates were used to prepared MOF-covered electrodes: copper plate (thickness: 1 mm, 99% purity, Testas, Belgium), copper wire (diameter: 1.5 mm) and copper foam (thickness: 1 mm, pore density: 90 ppi, Cu>99.5%, Changsha LYRUN New Material China Co., Ltd.). Before electrodeposition, the copper substrate was carefully cleaned with dilute hydrochloric acid, acetone and ultrapure water several times, respectively. Unless stated otherwise, the anodic MOF deposition was

performed on different kinds of copper substrates under the same conditions. Copper plates were used as the cathode, and different copper substrates were used as the anode. The electrodeposition was performed in a solution containing 1 g 1,3,5-benzenetricarboxylic acid ($H_3BTC$) and 0.5 g methyltributylammonium methyl sulfate (MTBS) per 100 mL solvent (67 mL ethanol and 33 mL Milli-Q® water). By applying a current density of 4 mA $cm^{-2}$ at room temperature until the total passed charge reached 36 C $cm^{-2}$, MOFs were grown on the copper substrates. The current densities were determined by geometric area. After MOF growth, the MOF-covered electrode was washed with ethanol and dimethylformamide (DMF) to remove excess ligand and MTBS.

*Preparation of Cu@porous carbon matrix electrode*: The MOF-covered copper foam electrodes were pyrolized at 850 °C in flowing argon gas (99.998%) with a flow rate of 300 $cm^3$ $min^{-1}$. The temperature inside the furnace was gradually increased from room temperature to the target temperature at a heating rate of 3 °C $min^{-1}$. After the target temperature was reached, the MOF-covered copper foam electrode was annealed for 8 h and then cooled down to room temperature at a rate of 5 °C $min^{-1}$. The as-prepared electrode was denoted as Cu@porous carbon matrix electrode. For comparison, a copper plate and a copper foam were used as control samples.

*Material characterizations*: X-ray diffraction (XRD) data of the samples were collected on a Bruker AXS D8 diffractometer using Cu $K_\alpha$ radiation (wavenumber $\lambda$ = 0.15405 nm) and Ni filter from 5° to 50° in 2θ with a step of 0.02° (2 s per step). TGA was performed in an argon atmosphere on a thermogravimetric analyzer (AutoTGA 2950HR V5.4A, TA Instruments) using platinum pans at a heating rate of 3 °C $min^{-1}$. For the XRD and TGA tests, the sample was scratched off from the copper substrate. The morphology of the samples and energy dispersive spectroscopy (EDS) were observed on a FEI/Philips XL30 FEG microscope (SEM). In order to improve the electronic conductivity of the MOF samples, a 5 nm layer of Pt was sputtered on top of the samples. The onset temperature of the weight loss in the TGA was

used as the decomposition temperature ($T_d$). High resolution transmission electron microscopy (HRTEM) and scanning transmission electron microscopy (STEM) images were obtained by using an FEI Tecnai F20 field emission gun microscope operated at 200 kV with a point-to-point resolution of 0.19 nm, which is equipped with high angle annular dark field (HAADF) and electron energy loss spectroscopy (EELS) detectors The obtained images and spectra have been analyzed by means of Gatan Digital Micrograph software.

*Electrochemical characterizations*: The electrochemical performance of the samples was characterized by chronoamperometry (*i*-*t*) and cyclic voltammetry (CV) techniques with an Autolab electrochemical workstation at room temperature in a three-electrode system. The as-prepared electrode, platinum gauze and an Hg/HgO electrode were used as the working electrode, the counter electrode and the reference electrode, respectively. The working electrode was used after being activated for several cycles of cyclic voltammetry form 0 to 0.65V at a scan rate of 50 mV $s^{-1}$ until CV curves are stable. The supporting electrolyte in all electrochemical experiments is 0.1 M NaOH.

Acknowledgements

X. Zhang is grateful to China Scholarship Council. Financial support from China Fund KU Leuven (ISP/13/02SJT) is acknowledged. J. Luo acknowledges the Research Foundation - Flanders (FWO) for a FWO Postdoctoral Fellowship (12F5514N), a Research Grant (Project number: 1529816N) and a travel grant (V410316N) for a Visiting Professorship at the Technical University of Denmark. JA, PYT and JRM acknowledge funding from Generalitat de Catalunya 2014 SGR 1638 and the Spanish MINECO coordinated projects between IREC and ICN2 TNT-FUELS and e-TNT (MAT2014-59961-C2-2-R). ICN2 acknowledges support from the Severo Ochoa Program (MINECO, Grant SEV-2013-0295). Part of the present work has been performed in the framework of Universitat Autonoma de Barcelona Materials Science Ph.D. program.

Received: ((will be filled in by the editorial staff))
Revised: ((will be filled in by the editorial staff))
Published online: ((will be filled in by the editorial staff))

**References**


1. Fisher, K.; Griffith, L.; Gruneir, A.; Panjwani, D.; Gandhi, S.; Sheng, L.; Gafni, A.; Chris, P.; Markle-Reid, M.; Ploeg, J., Comorbidity and its relationship with health service use and cost in community-living older adults with diabetes: A population-based study in Ontario, Canada. Diabetes Research and Clinical Practice 2016, 122, 113-123.
2. Wang, G.; He, X.; Wang, L.; Gu, A.; Huang, Y.; Fang, B.; Geng, B.; Zhang, X., Non-enzymatic electrochemical sensing of glucose. *Microchimica Acta* **2012,** *180* (3-4), 161–186.
3. Wang, J., Electrochemical glucose biosensors. *Chemical Reviews* **2008,** *108* (2), 814–825.
4. Zaidi, S. A.; Shin, J. H., Recent developments in nanostructure based electrochemical glucose sensors. *Talanta* **2016,** *149*, 30–42.
5. Feng, D.; Wang, F.; Chen, Z., Electrochemical glucose sensor based on one-step construction of gold nanoparticle-chitosan composite film. *Sensors and Actuators B: Chemical* **2009,** *138* (2), 539–544;
6. Guo, C.; Zhang, X.; Huo, H.; Xu, C.; Han, X., $Co_3O_4$ microspheres with free-standing nanofibers for high performance non-enzymatic glucose sensor. *The Analyst* **2013,** *138* (22), 6727–6731.
7. Lu, W.; Qin, X.; Asiri, A. M.; Al-Youbi, A. O.; Sun, X., Ni foam: a novel three-dimensional porous sensing platform for sensitive and selective nonenzymatic glucose detection. *The Analyst* **2013,** *138* (2), 417–420.
8. Qian, L.; Mao, J.; Tian, X.; Yuan, H.; Xiao, D., In situ synthesis of CuS nanotubes on Cu electrode for sensitive nonenzymatic glucose sensor. *Sensors and Actuators B: Chemical* **2013,** *176*, 952–959.
9. Ren, X.; Meng, X.; Chen, D.; Tang, F.; Jiao, J., Using silver nanoparticle to enhance current response of biosensor. *Biosensors & Bioelectronics* **2005,** *21* (3), 433–437.
10. Wei, H.; Wang, E., $Fe_3O_4$ magnetic nanoparticles as peroxidase mimetics and their applications in $H_2O_2$ and glucose detection. *Analytical Chemistry* **2008,** *80* (6), 2250–2254.
11. Yuan, J.; Cen, Y.; Kong, X. J.; Wu, S.; Liu, C. L.; Yu, R. Q.; Chu, X., $MnO_2$-Nanosheet-Modified Upconversion Nanosystem for Sensitive Turn-On Fluorescence Detection of $H_2O_2$ and Glucose in Blood. *ACS Applied Materials & Interfaces* **2015,** *7* (19), 10548–10555.
12. Zhai, D.; Liu, B.; Shi, Y.; Pan, L.; Wang, Y.; Li, W.; Zhang, R.; Yu, G., Highly sensitive glucose sensor based on Pt nanoparticle/polyaniline hydrogel heterostructures. *ACS Nano* **2013,** *7* (4), 3540–3546.
13. Huang, J.; Zhu, Y.; Yang, X.; Chen, W.; Zhou, Y.; Li, C., Flexible 3D porous CuO nanowire arrays for enzymeless glucose sensing: in situ engineered versus ex situ piled. *Nanoscale* **2015,** *7* (2), 559–569.
14. Meher, S. K.; Rao, G. R., Archetypal sandwich-structured CuO for high performance non-enzymatic sensing of glucose. *Nanoscale* **2013,** *5* (5), 2089–2099.
15. Huang, T. K.; Lin, K. W.; Tung, S. P.; Cheng, T. M.; Chang, I. C.; Hsieh, Y. Z.; Lee, C. Y.; Chiu, H. T., Glucose sensing by electrochemically grown copper nanobelt electrode. *Journal of Electroanalytical Chemistry* **2009,** *636* (1-2), 123–127.
16. Kang, X.; Mai, Z.; Zou, X.; Cai, P.; Mo, J., A sensitive nonenzymatic glucose sensor in alkaline media with a copper nanocluster/multiwall carbon nanotube-modified glassy carbon electrode. *Analytical Biochemistry* **2007,** *363* (1), 143–150.
17. Xu, Q.; Zhao, Y.; Xu, J. Z.; Zhu, J. J., Preparation of functionalized copper nanoparticles and fabrication of a glucose sensor. *Sensors and Actuators B: Chemical* **2006,** *114* (1), 379–386.
18. Yang, J.; Zhang, W. D.; Gunasekaran, S., An amperometric non-enzymatic glucose sensor by electrodepositing copper nanocubes onto vertically well-aligned multi-walled carbon nanotube arrays. *Biosensors & bioelectronics* **2010,** *26* (1), 279–284.
19. Zhang, L.; Zhang, J.; Yang, C.; Zhao, G.; Mu, J.; Wang, Y., Freestanding Cu nanowire arrays on Ti/Cr/Si substrate as tough nonenzymatic glucose sensors. *RSC Adv.* **2015,** *5* (101),

82998–83003.
20. Jiang, D.; Liu, Q.; Wang, K.; Qian, J.; Dong, X.; Yang, Z.; Du, X.; Qiu, B., Enhanced non-enzymatic glucose sensing based on copper nanoparticles decorated nitrogen-doped graphene. *Biosensors & Bioelectronics* **2014,** *54*, 273–278.
21. Ahmad, R.; Tripathy, N.; Jung, D. U.; Hahn, Y. B., Highly sensitive hydrazine chemical sensor based on ZnO nanorods field-effect transistor. *Chemical Communications* **2014,** *50* (15), 1890–1893.
22. Jia, W.; Guo, M.; Zheng, Z.; Yu, T.; Wang, Y.; Rodriguez, E. G.; Lei, Y., Vertically Aligned CuO Nanowires Based Electrode for Amperometric Detection of Hydrogen Peroxide. *Electroanalysis* **2008,** *20* (19), 2153–2157.
23. Sun, S.; Zhang, X.; Sun, Y.; Yang, S.; Song, X.; Yang, Z., Facile water-assisted synthesis of cupric oxide nanourchins and their application as nonenzymatic glucose biosensor. *ACS Applied Materials & Interfaces* **2013,** *5* (10), 4429–4437.
24. Li, Z.; Chen, Y.; Xin, Y.; Zhang, Z., Sensitive electrochemical nonenzymatic glucose sensing based on anodized CuO nanowires on three-dimensional porous copper foam. *Scientific Reports* 2015, 5, 16115–16123.
25. Bak, W.; Kim, H. S.; Chun, H.; Yoo, W. C., Facile synthesis of metal/metal oxide nanoparticles inside a nanoporous carbon matrix (M/MO@C) through the morphology-preserved transformation of metal-organic framework. *Chemical Communications* **2015,** *51* (33), 7238–7241.
26. Liu, J.; Wang, H.; Wu, C.; Zhao, Q.; Wang, X.; Yi, L., Preparation and characterization of nanoporous carbon-supported platinum as anode electrocatalyst for direct borohydride fuel cell. *International Journal of Hydrogen Energy* **2014,** *39* (12), 6729–6736.
27. Pandiaraj, S.; Aiyappa, H. B.; Banerjee, R.; Kurungot, S., Post modification of MOF derived carbon via g-$C_3N_4$ entrapment for an efficient metal-free oxygen reduction reaction. *Chemical Communications* **2014,** *50* (25), 3363–3366.
28. Wei, C.; Li, X.; Xu, F.; Tan, H.; Li, Z.; Sun, L.; Song, Y., Metal organic framework-derived anthill-like Cu@carbon nanocomposites for nonenzymatic glucose sensor. *Analytical Methods* **2014,** *6* (5),1550–1557.
29. Yue, H.; Shi, Z.; Wang, Q.; Cao, Z.; Dong, H.; Qiao, Y.; Yin, Y.; Yang, S., MOF-derived cobalt-doped ZnO@C composites as a high-performance anode material for lithium-ion batteries. *ACS Applied Materials & I–nterfaces* **2014,** *6* (19), 17067–17074.
30. Zhang, P.; Sun, F.; Xiang, Z.; Shen, Z.; Yun, J.; Cao, D., ZIF-derived in situ nitrogen-doped porous carbons as efficient metal-free electrocatalysts for oxygen reduction reaction. *Energy & Environmental Science* **2014,** *7* (1), 442–450.
31. Zhang, X.; Luo, J.; Tang, P.; Ye, X.; Peng, X.; Tang, H.; Sun, S. G.; Fransaer, J., A universal strategy for metal oxide anchored and binder-free carbon matrix electrode: A supercapacitor case with superior rate performance and high mass loading. *Nano Energy* **2017,** *31*, 311–321.
32. U. Mueller, H. Putter, M. Hesse, M. Schubert, H. Wessel, J. Huff and M. Guzmann, US Pat. 2007/0227898 A1, **2007**.
33. Ameloot, R.; Stappers, L.; Fransaer, J.; Alaerts, L.; Sels, B. F.; De Vos, D. E., Patterned Growth of Metal-Organic Framework Coatings by Electrochemical Synthesis. *Chemistry of Materials* **2009,** *21* (13), 2580–2582.
34. Campagnol, N.; Van Assche, T. R. C.; Li, M.; Stappers, L.; Dincă, M.; Denayer, J. F. M.; Binnemans, K.; De Vos, D. E.; Fransaer, J., On the electrochemical deposition of metal–organic frameworks. J. Mater. Chem. A 2016, 4 (10), 3914–3925.
35 Campagnol, N.; Van Assche, T.; Boudewijns, T.; Denayer, J.; Binnemans, K.; De Vos, D.; Fransaer, J., High pressure, high temperature electrochemical synthesis of metal–organic frameworks: films of MIL-100 (Fe) and HKUST-1 in different morphologies. *Journal of Materials Chemistry A* **2013,** *1* (19), 5827–5830.

36. Kim, S. S.; Na, H. G.; Choi, S. W.; Kwak, D. S.; Kim, H. W., Novel growth of CuO-functionalized, branched $SnO_2$nanowires and their application to $H_2S$ sensors. *Journal of Physics D: Applied Physics* **2012,** *45* (20), 205301–8.
37. Zhang, X.; Wang, L.; Liu, C.; Ding, Y.; Zhang, S.; Zeng, Y.; Liu, Y.; Luo, S., A bamboo-inspired hierarchical nanoarchitecture of Ag/CuO/$TiO_2$ nanotube array for highly photocatalytic degradation of 2,4-dinitrophenol. *Journal of Hazardous Materials* **2016,** *313*, 244–252.
38.Verbeeck, J.; Van Aert, S., Model based quantification of EELS spectra. *Ultramicroscopy* **2004,** *101* (2-4), 207–224.
39. Keil, P.; Lützenkirchen‐Hecht, D.; Frahm, R.; Hedman, B.; Pianetta, P. In Investigation of Room Temperature Oxidation of Cu in Air by Yoneda‐XAFS, AIP Conference Proceedings, AIP: 2007; 490–492.
40. Sun, S.; Zhang, X.; Sun, Y.; Zhang, J.; Yang, S.; Song, X.; Yang, Z., A facile strategy for the synthesis of hierarchical CuO nanourchins and their application as non-enzymatic glucose sensors. *RSC Advances* **2013**, 3 (33), 13712–13719.
41. Kong, C.; Tang, L.; Zhang, X.; Sun, S.; Yang, S.; Song, X.; Yang, Z., Templating synthesis of hollow CuO polyhedron and its application for nonenzymatic glucose detection. *Journal of Materials Chemistry A* **2014,** *2* (20), 7306–7312;
42. Li, K.; Fan, G.; Yang, L.; Li, F., Novel ultrasensitive non-enzymatic glucose sensors based on controlled flower-like CuO hierarchical films. *Sensors and Actuators B: Chemical* **2014,** *199*, 175–182.
43. Zhang, Y.; Su, L.; Manuzzi, D.; de los Monteros, H. V.; Jia, W.; Huo, D.; Hou, C.; Lei, Y., Ultrasensitive and selective non-enzymatic glucose detection using copper nanowires. *Biosensors & Bioelectronics* **2012,** *31* (1), 426–432.
44. Li, H.; Guo, C. Y.; Xu, C. L., A highly sensitive non-enzymatic glucose sensor based on bimetallic Cu-Ag superstructures. *Biosensors & Bioelectronics* **2015,** *63*, 339–346.

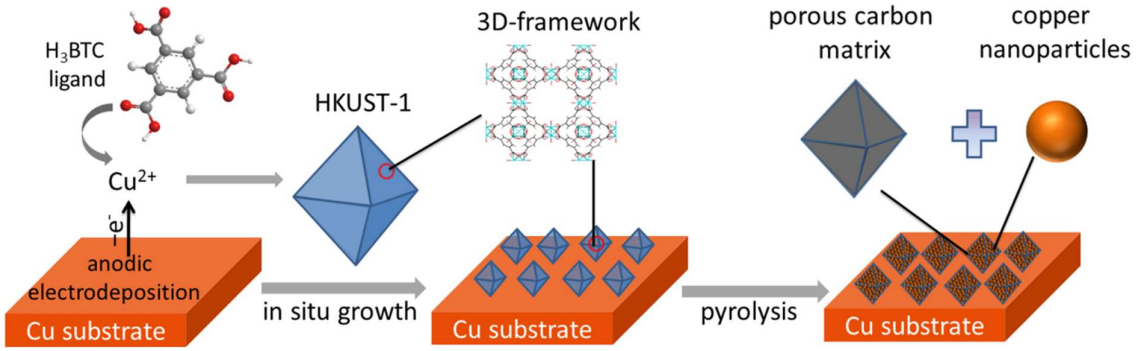


**Figure 1**. Schematic illustration of the synthesis of Cu@porous carbon matrix on the copper foam substrates.

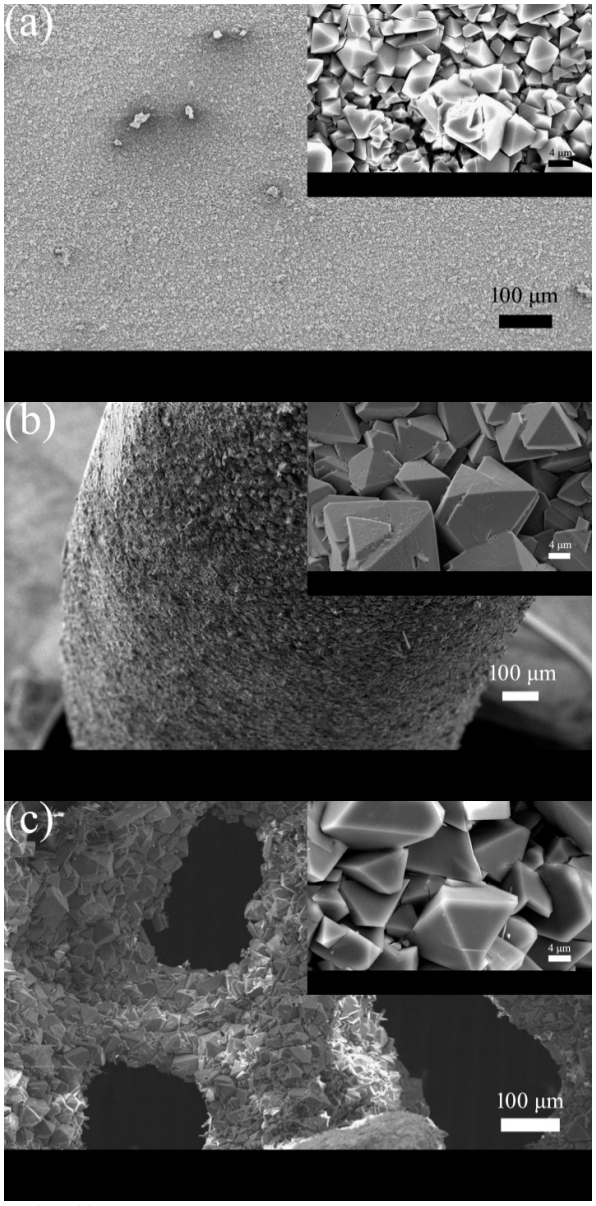


**Figure 2**. SEM images of different MOF-covered copper substrates: (a) copper plate; (b) copper wire and (c) copper foam. Insets are the corresponding magnifications with a scale bar of 4 μm.

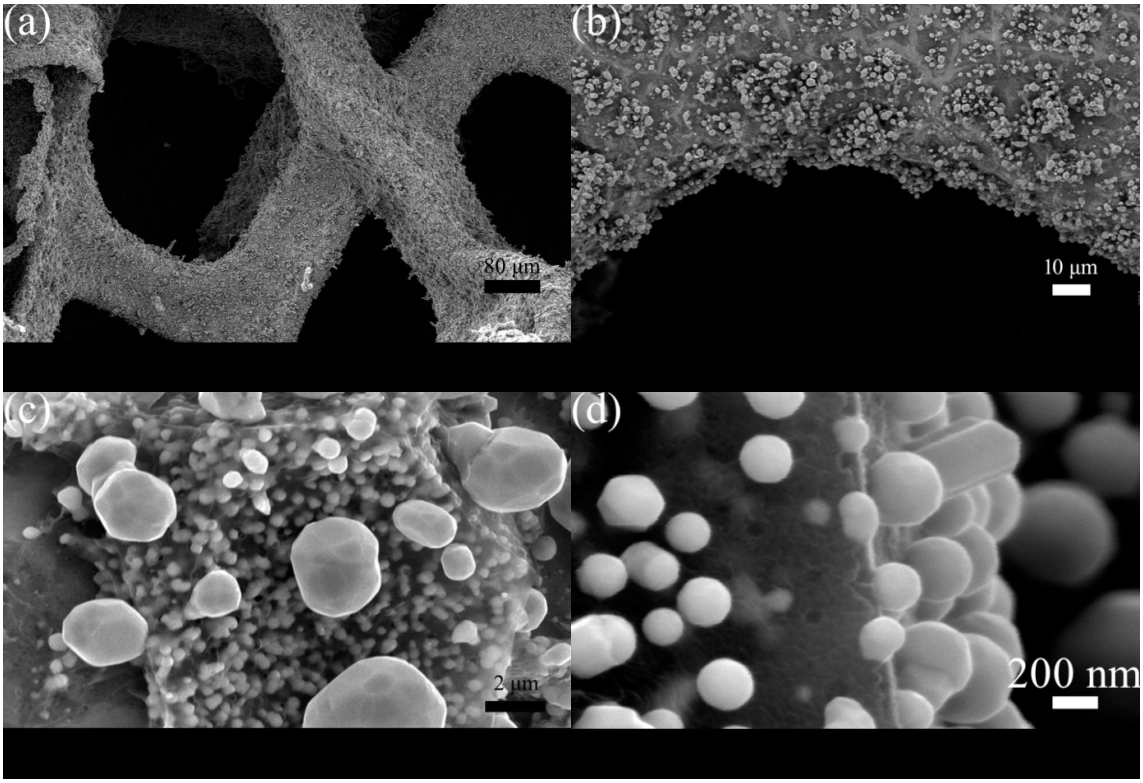


**Figure 3**. SEM images of the Cu@porous carbon matrix electrode at different magnifications. The scale bars are (a) 80 µm (b) 10 µm, (c) 2 µm and (d) 200 nm, respectively.

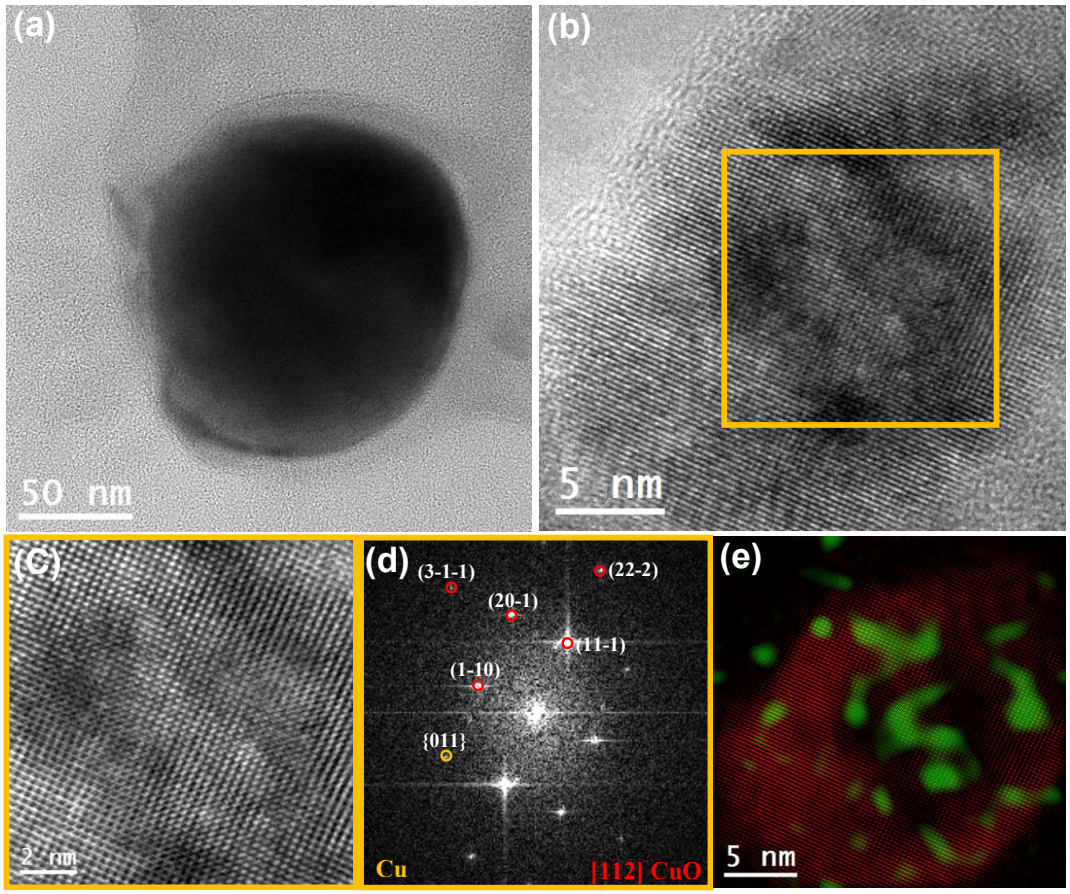


**Figure 4.** TEM images of Cu@porous carbon matrix materials (removed from the Cu foam) at the resolution of 50 nm (a) and 5 nm (b), respectively. (c) Details of the region squared in yellow and (d) the corresponding indexed power spectrum. (e) The RGB composition of IFFT from CuO (red) and Cu (green).

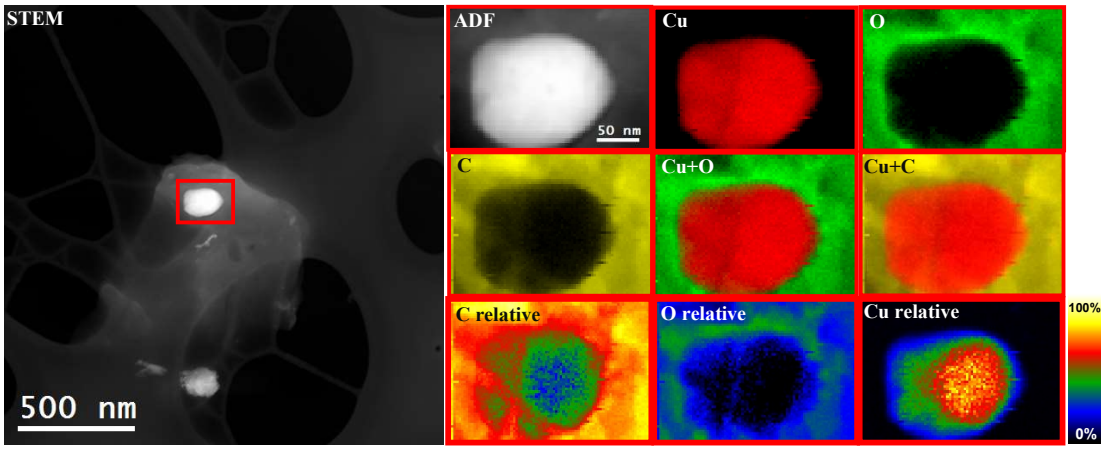


**Figure 5**. EELS chemical composition maps of Cu@porous carbon matrix materials (removed from the Cu foam) obtained from the area squared in red on the ADF-STEM micrograph. Right top and right middle: Individual Cu (red), O (green), C (yellow) maps and their composites; Right bottom: the relative composition map of C, O and Cu elements.

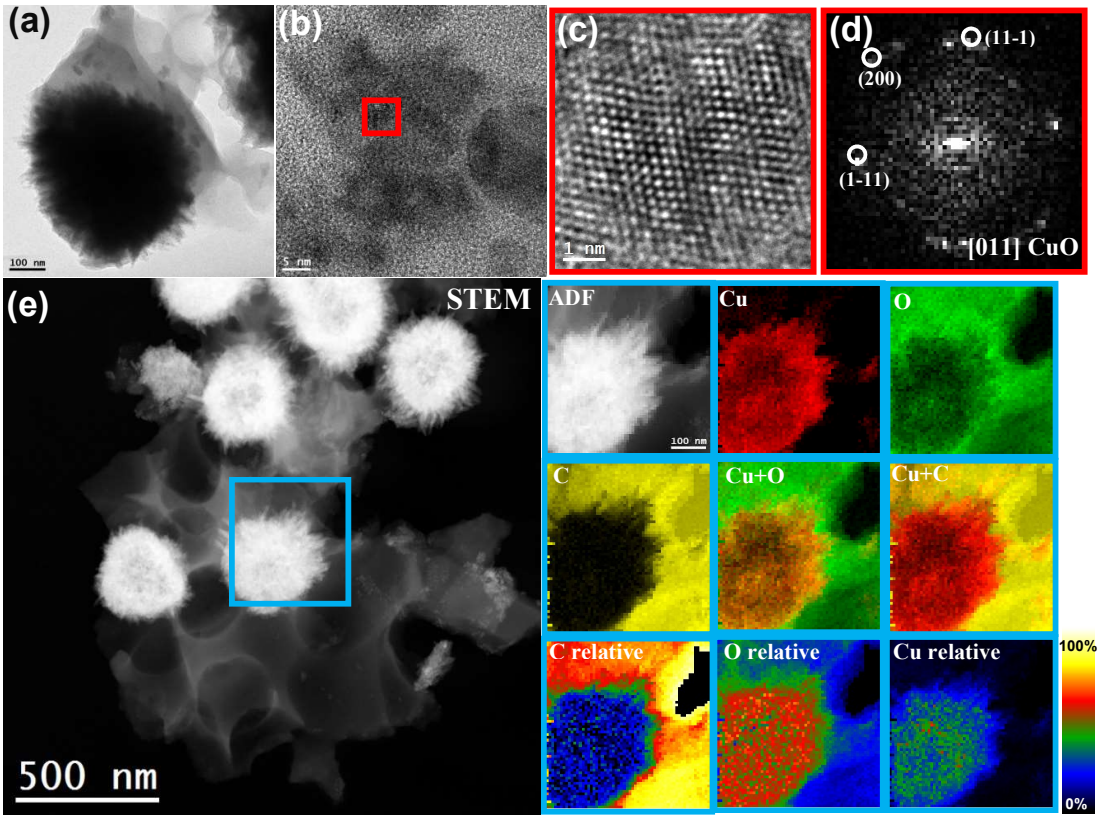


**Figure 6**. (a) and (b) TEM images of Cu@porous carbon matrix materials after sensor test (removed from the Cu foam). (c) details of the squared region in red line and (d) their corresponding indexed power spectrum. (e) EELS chemical composition maps of Cu@porous carbon matrix materials after glucose sensor test (scratched from Cu foam) obtained from the area squared in indigo on the ADF-STEM micrograph. Right top and right middle: Individual Cu (red), O (green), C (yellow) maps and their composites; Right bottom: the relative composition map of C, O and Cu elements.

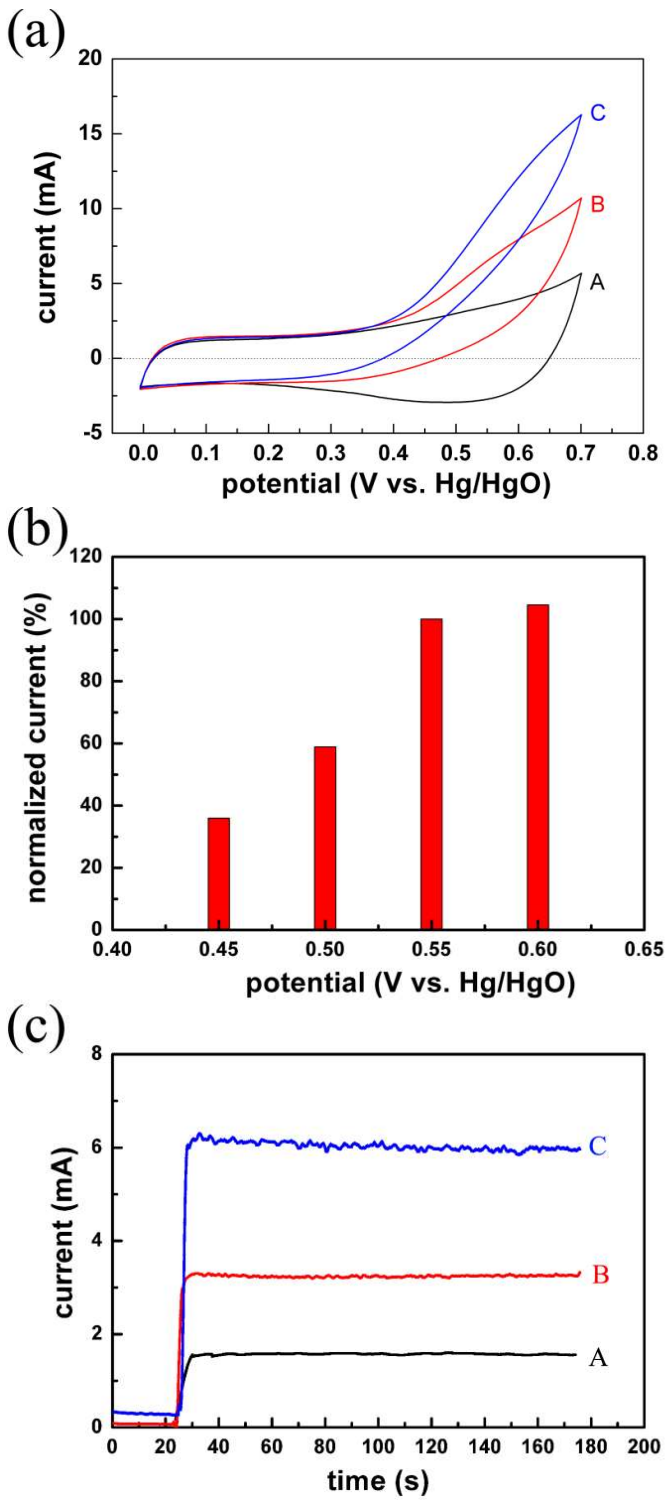


**Figure 7**. (a) CV curves of Cu@porous carbon matrix electrode in the absence (A) and presence of glucose (B: 1 mM glucose; C: 2 mM glucose) at a scan rate of 50 mV $s^{-1}$, respectively. (b) Amperometric responses of Cu@porous carbon matrix electrode at potentials from +0.45 V to +0.6 V vs. Hg/HgO to the addition of 1 mM glucose (normalized by the amperometric response at +0.55 V vs. Hg/HgO). (c) Amperometric responses of the copper plate electrode (A), copper foam electrode (B) and Cu@porous carbon matrix electrode (C) to the addition of 1 mM glucose at +0.55 V vs. Hg/HgO.

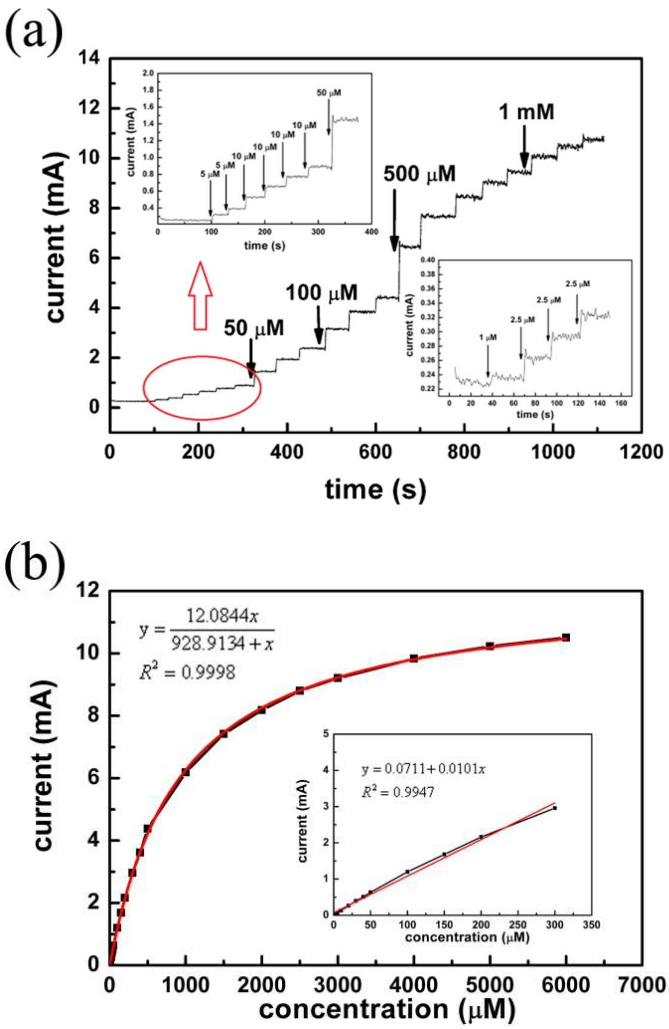


**Figure 8**. (a) Amperometric response of the Cu@porous carbon matrix electrode to successive additions of increased concentrations of glucose solutions to 0.1 M NaOH solution at an applied potential of +0.55 V (*vs*. Hg/HgO). The low-concentration part is magnified and shown in the inset in the upper left corner. The inset curve in the lower right corner is amperometric response of Cu@porous carbon matrix electrode to successive addition of glucose solution with smaller concentrations. (b) Corresponding calibration curve for **Figure 8 (a)**.

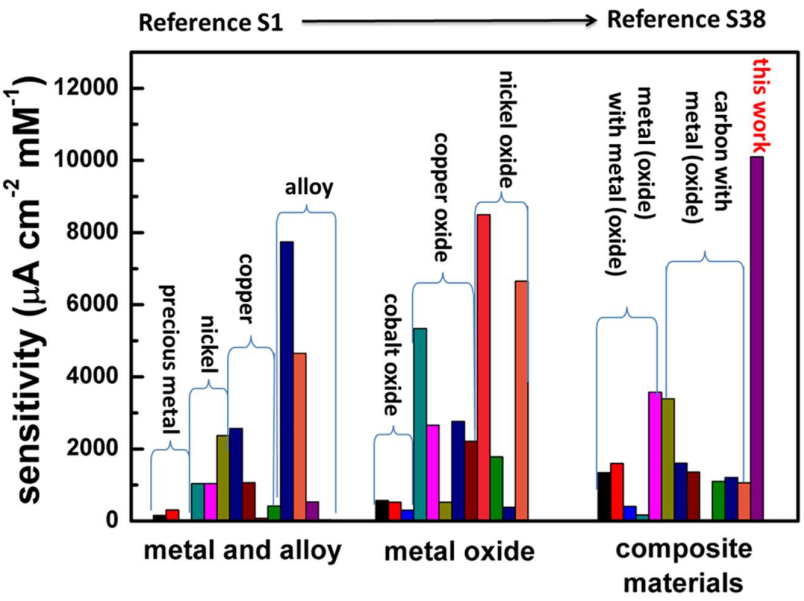


**Figure 9.** Comparison of the sensitivity of Cu@porous carbon matrix electrode with other electrodes reported in the literature (the related references S1~S38 are listed in the supplementary information).

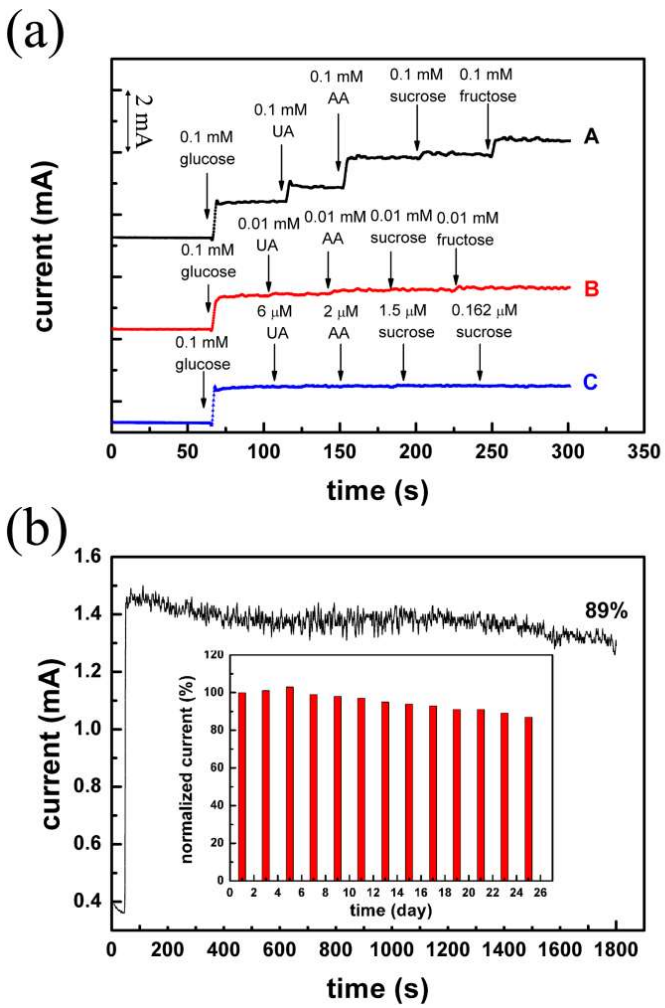


**Figure 10**. (a) The selectivity study of Cu@porous carbon matrix electrode with addition of different concentrations of UA, AA, sucrose, fructose and glucose at an applied potential of +0.55 V. (b) Long term stability of Cu@porous carbon matrix electrode at +0.55 V for 1800 s. Inset shows the normalized sensitivity of Cu@porous carbon matrix electrode to glucose tested every two days by amperometric measurement over 25 consecutive days.